A Study of Frontal Cyclone Surface and 300-hPa Geostrophic Kinetic Energy Distribution and Scale Change

RICHARD GROTJAHN AND CRIS CASTELLO

Atmospheric Science Program, Department of Land, Air, and Water Resources, University of California, Davis, Davis, California

(Manuscript received 3 March 1999, in final form 16 November 1999)

ABSTRACT

An earlier article deduced a doubling of the scale of the sea level pressure pattern for lows as they developed in the North Pacific. Scale here refers to horizontal extent of the low. This study uses a different technique to estimate scale change in the upper troposphere. The prior study used wavelets; here circular averaging is used on several fields, with primary emphasis on the geostrophic kinetic energy (gKE) field.

The technique herein confirms the earlier result that sea level pressure (SLP) scale increases. When applied to the 300-hPa level, the trough extent does not change scale significantly. The average scale has radius of about 1200 km at sea level and 1700 km at 300 hPa. During development the average radius of maximum gKE changes little at the surface but decreases at upper levels. The maximum gKE is typically located 600–1100 km from the 300-hPa low center, 450–650 km from the SLP low center. Composite maps of gKE are shown during different stages in cyclone development at both levels. Consistency between the results presented here and the conventional view of jet streak migration around an upper low is mentioned. Some implications for theoretical work are mentioned.

1. Introduction

In Grotjahn (1996a) the evolution of each trough axis for 27 western North Pacific frontal cyclones was examined. Grotjahn (1996b) looked in detail at the composite structure and vorticity equation terms in 15 of those 27 cyclones (which shared the most similar structure at the mature stage). This study and Grotjahn et al. (1999, hereafter GHC) consider 12 of those 15 cases. The 12 frontal cyclones are chosen in order to assess changes in their widths throughout their developmental stages. GHC applied wavelet analysis to the sea level pressure fields at each 12-h time interval in order to obtain an objective method for measuring changes in the cyclones' horizontal scale. Scale as used here refers to the horizontal extent of the low. GHC's main conclusion was that the average diameter of the lows doubles over a 4-day period. This paper looks at the 300-hPa geopotential height patterns above those 12 surface cyclones and attempts to discern a scale change in the corresponding upper-level troughs. The 12 cases are listed in Table 1.

The wavelet analysis technique worked for sea level data but does not work at upper levels. Reasons for developing a different technique are outlined in the next section. Circularly averaged geostrophic kinetic energy (gKE) provided a satisfactory parameter to assess each storm's scale. In section 3, horizontal distribution and scale changes of the gKE field are discussed. The final section briefly summarizes the main results.

2. Analysis technique

a. Background

Various methods for obtaining a suitable measurement of the 300-hPa trough scale were applied. These are summarized to provide context for the technique we ultimately used. In short, the method used in GHC at the surface fails when applied to the two-dimensional fields at higher levels. Various extensions of this approach also fail, whereas a straightforward technique based on circular averaging works satisfactorily.

GHC used wavelet analysis in both the meridional and zonal directions. Wavelet analysis was successfully applied to the sea level pressure (SLP) field because SLP has a cellular pattern.

Wavelet analysis was unsuitable for the upper-level geopotential fields for several reasons. The first problem arises from the strong meridional trend in these fields. Standard wavelet analysis removes the mean across the data. Directly applying wavelet analysis in the meridi-

Corresponding author address: Prof. Richard Grotjahn, Atmospheric Science Program, University of California, Davis, Hoagland Hall, One Shields Avenue, Davis, CA 95616-8627.
E-mail: grotjahn@ucdavis.edu

TABLE 1. Starting and ending times used and central pressure at the normalization time for the 12 frontal cyclones.*

Case letter	Case no. (yr month day)	Starting time	Ending time	Central pressure (hPa)
A	93 1211	1200 UTC 09 Dec 1993	1200 UTC 13 Dec 1993	989.7
B	94 0114	0000 UTC 13 Jan 1994	1200 UTC 16 Jan 1994	990.0
C	94 0129	1200 UTC 27 Jan 1994	0000 UTC 31 Jan 1994	995.6
D	94 0209	1200 UTC 07 Feb 1994	1200 UTC 11 Feb 1994	985.9
E	90 0107	0000 UTC 05 Jan 1990	0000 UTC 09 Jan 1990	999.8
F	90 1226	1200 UTC 24 Dec 1990	0000 UTC 28 Dec 1990	996.5
G	91 0118	1200 UTC 16 Jan 1991	1200 UTC 20 Jan 1991	992.1
H	92 0117	0000 UTC 16 Jan 1992	1200 UTC 19 Jan 1992	998.9
I	92 0201	0000 UTC 30 Jan 1992	0000 UTC 03 Feb 1992	983.9
J	92 0224	1200 UTC 22 Feb 1992	1200 UTC 26 Feb 1992	983.9
K	91 1228	0000 UTC 26 Dec 1991	0000 UTC 30 Dec 1991	990.2
L	91 0212	0000 UTC 10 Feb 1991	0000 UTC 14 Feb 1991	988.9

* Table corrects minor errors in the corresponding table in GHC.

onal direction is unsuitable: the analysis simply selects the hemisphere as the primary length scale. Removing the zonal mean results in a perturbation field that has a somewhat cellular pattern that at first glance appears suitable for wavelet analysis in both directions. However, the wavelet analysis was inconclusive due to a second problem: the resulting cellular pattern was very asymmetric. In contrast, the Mexican hat mother wavelet used by GHC is symmetric. The wavelet analysis often found a peak wavelet (having largest amplitude in the spectrum) that was obviously very different in scale than the observed feature.

Other mother wavelets exist that are asymmetric. However, no attempt was made to use such wavelets because (a) the familiar ones had too great an asymmetry and (b) the asymmetry in our data was not consistent between cases or even within a case over time. To summarize the various patterns seen: the trailing and leading highs were often different in amplitude and in proximity to the low. Simple dynamical reasoning leads one to expect the upper-level ridge to lie ahead of the surface low and to be built by the warm air advection and latent heating of the rising air. Such an upper ridge usually greatly exceeds any ridge that might trail the upper trough when the trough has large amplitude (at later times in the sequence). Also, that ridge would be connected more strongly to the trough than would any ridge behind the trough. Hence, the leading ridge was closer than the trailing ridge, sometimes much closer. These features are seen in the example plotted in Fig. 1. In contrast, prior to development either high could be the stronger (or closer) of the two when the trough was weak.

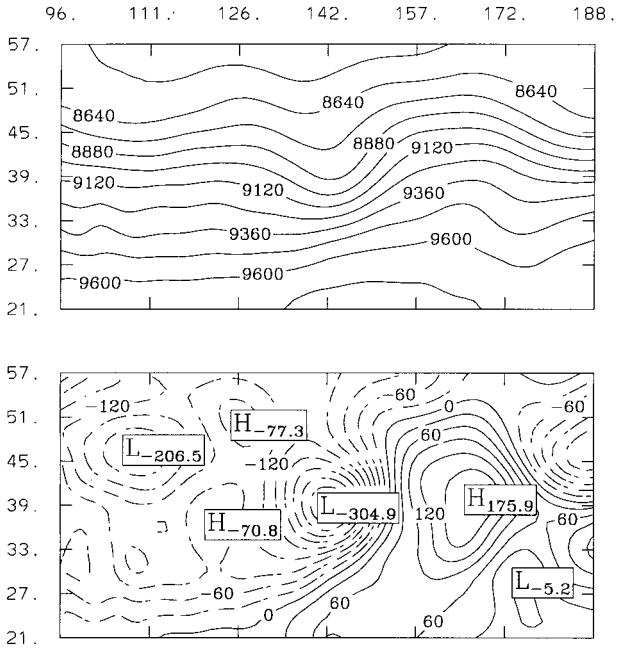

FIG. 1. A sample comparison of full (upper) and perturbation (lower plot) geopotential height fields at 300 hPa at day = 0 (time sample 5) for case A. See Table 1. Contour interval: (a) 120 m and (b) 30 m.

Wavelet analysis was attempted with other fields. Geostrophic relative vorticity has a somewhat cellular pattern. However, at upper levels there is horizontal shear vorticity from the larger-scale jet stream that was difficult to remove. The curvature portion of the vorticity field was unsuitable since that field was extremely noisy and a suitable wavelet with a similar shape could not be found. Working with the inverse curvature was equally inconclusive. (The radius of curvature, R, goes to zero at the center of a cyclone, so $1/R$ goes to infinity.)

An alternative to using wavelet analysis is using a simple least squares fit to a known function whose scale is known. Using a zonal slice through the center of each low, a sinusoidal curve was fit to the (zonal deviation) height pattern. A least squares algorithm was used to find the best fit to the data. This method failed for various reasons. For one, the asymmetric nature of the data around the trough conflicted with the symmetric nature of a sinusoidal curve around its peaks and valleys. In particular, when one side of the perturbation trough was steeper than the other, a sinusoidal fit was a poor match. Also, there were problems during the early stages of the

trough development; when the nascent trough was embedded within a larger, more prominent trough, the least squares fit would choose too large a sinusoidal wave in an attempt to fit it to the larger background trough.

b. Circular averaging

As detailed above, attempts to use symmetric patterns to fit the trough shapes failed to work satisfactorily. This is not to say that the perturbation troughs obtained were all that asymmetric. Instead, the breakdown of each method was often caused by nearby structures that were asymmetrically distributed relative to the lows. This realization suggested a much simpler approach: to define the scale from a circular average using a coordinate frame centered on the trough. The goal is to find one scale for a conceptually circular trough, so, it is reasonable to define that scale from a circular average.

Each 300-hPa geopotential perturbation field was obtained by subtracting a zonal sector mean from the total 300-hPa field. The zonal mean was calculated over the sector from 72°E through 114°W. This 300-hPa geopotential perturbation field had a cellular pattern of highs and lows and hence provided an objective way of defining the ''center'' of each low. As discussed in Grotjahn (1996a) perturbations defined by subtracting off the zonal mean around an entire latitude circle do not produce reasonable highs and lows. Problems occur because the large-amplitude highs and lows tend to occur at different latitudes and because the jet streams vary in strength and location. In Grotjahn (1996a) individual lows were isolated by removing a ''background'' field defined using bilinear interpolation over a small domain centered on each trough; the procedure was extremely laborious since one needed to choose a domain that was suitable for all levels. Only one level was considered in this study and the cases chosen generally have subjectively reasonable perturbation height patterns by using the indicated fixed domain. Figure 1 shows a typical example.

The gKE and geostrophic vorticity fields were obtained from the perturbation geopotential field. The gKE field has several advantages over the vorticity field. The main advantage is that scale is less ambiguous for the gKE field. At the cyclone center gKE goes to zero; it also decreases to a background level at some distance from the cyclone. In between, gKE has a maximum. This pattern holds at the surface and at upper levels, thus allowing some comparison with the earlier study. A further advantage of using gKE is that the scale may be defined from the energy contained within the cyclone, arguably a more direct measure of the storm's extent than inferring extent from the pressure pattern. Nonetheless, Nielsen and Dole (1992) and GHC successfully deduced scale from the SLP fields. In contrast, inferring scale from upper-level geopotential height did not successfully infer storm scale but the perturbation gKE field did.

The method first calculated geostrophic kinetic energy at each grid point. Then a circle was defined having radius 3000 km from the center of the low in the perturbation height field. This distance was chosen to ensure capture of the gross features of any disturbance. Next, gKE was interpolated radially to every 50 km from the center of the low out to 3000 km. Thirty-six such radial cross sections were created, at 10° intervals around the circle. A two-dimensional quadratic scheme was used to interpolate the gridded data to these radial locations. The 36 radial data strings were then combined to create a circular average of kinetic energy as a function of radial distance from the perturbation low center.

National Centers for Environmental Prediction data in T42 spherical harmonic coefficients were transformed onto a high-resolution, T106 Gaussian grid. The Gaussian grid has approximately 1° resolution. The high-resolution grid was used to minimize finite-differencing inaccuracies. The T42 resolution is uniform over the globe with an approximately $\Delta = 125$ km interval. We tested analytic functions having a single isolated peak of various sizes; we determined that peaks with 3Δ radius above the cutoff value were sufficiently resolved. All of the scales found here exceed 500 km. Also, the smallest scales happen early in the development, when the 300-hPa troughs are over or near eastern Asia, a region of good upper-air observational coverage. Hence, we believe that the scales plotted are adequately resolved in the data.

Each cyclone was followed for nine consecutive times, which together define one case. Hence, there were nine such circular averages for each 300-hPa trough (one for each time step). Not surprisingly, most of the composites had these properties: being near zero at the center of the perturbed low, achieving a maximum at some distance from the center, then tailing off again.

The circular average gave a means to measure a scale associated with each time of each trough. A ''cutoff value''—a value of gKE that each circular average must exceed—determined which times were included in our final sample. Moving outward from the cyclone center (radius = 0) the scale was defined to be the point at which the average gKE equaled the cutoff value for a second time (that cutoff had been exceeded at a smaller radius). In essence, the scheme assumed that gKE below the cutoff value cannot be distinguished from gKE associated with nearby systems or with the background flow (on a circular average). This technique provided an objective means of identifying the bulk of each system. Further, this technique accommodated a wide range of asymmetry in the structure, both radially and annularly.

The average radial location of the maximum gKE was unsuitable for defining the scale change for several reasons. The primary reason concerned the deviation from circular symmetry that occured with the gKE maxima. Especially at early times prior to development, these maxima were isolated, elongated relative to the cyclone,

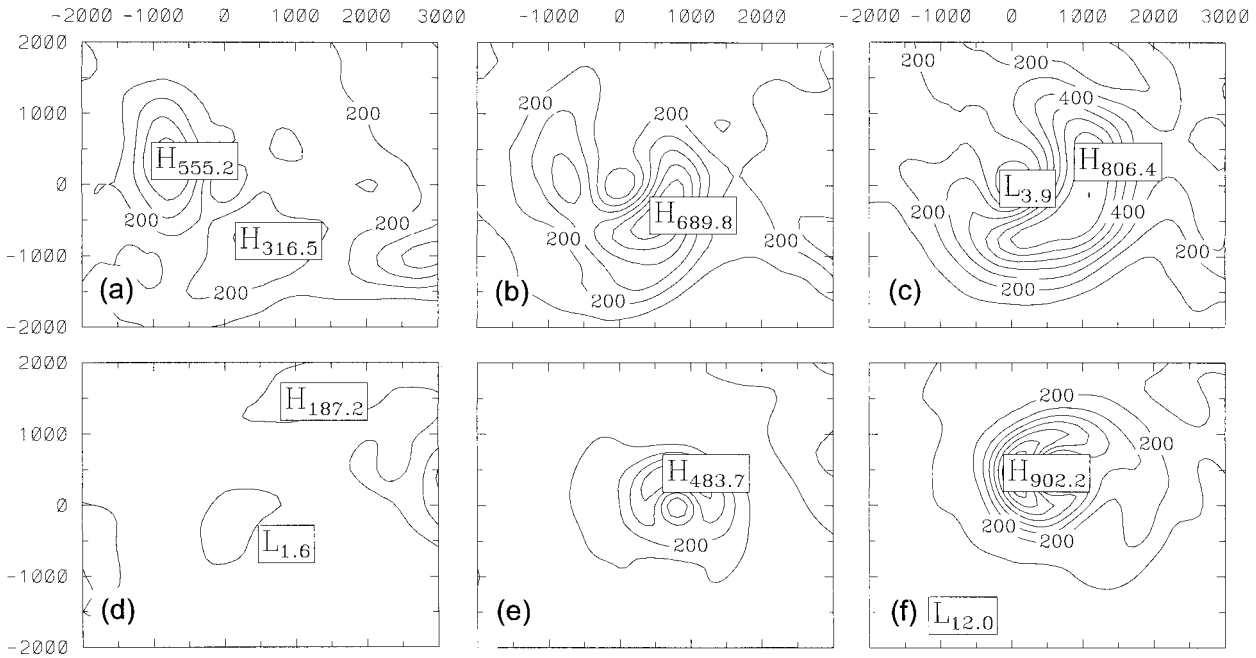

FIG. 2. Composite averages of gKE deduced from 300-hPa perturbation geopotential heights [upper row; (a)–(c)] and from sea level pressure [lower row; (d)–(f)] at three stages in the cyclones' development. Averages are calculated from 12 cyclones at times (a), (d) −1, (b), (e) 0, and (c), (f) +1.5 day for each storm. The zero hour was selected such that each storm has reached large amplitude but continues to grow for at least one more day and has been growing for at least one day. The relative locations of features at upper and lower levels were approximated here by shifting the origin in the plots of sea level gKE by the average amount for all cases relative to the 300-hPa low, after the composites are constructed. Contour interval 100 $m^2\ s^{-2}$.

and approached the cyclone center along a partly radial, partly tangential path. At later times there was often considerable circular symmetry in the strongest gKE values, but the location was closer to the low. Readers familiar with jet streaks can visualize this situation at upper levels. So, tracking the maximum in gKE mixed effects of scale change and structural change (i.e., shift of the jet streak location relative to the storm).

3. Results

a. General patterns of gKE

The scale change results are predicated on the distribution of the perturbation fields that remain after removal of a sector average. This study focuses on the perturbation geopotential height (Z) and corresponding gKE. The choice of sector was somewhat arbitrary. Readers should note that the zonal component of perturbation gKE has some dependency, but the meridional component is not dependent on the sector average chosen. However, if the sector average was problematical, then the perturbation gKE would favor certain regions; that problem was not visible in the 108 gKE fields calculated at 300 hPa. Instead, the fields were rather circularly symmetric and gKE maxima occurred in any quadrant. Figure 1 provides a sample comparison between the total and perturbation fields of Z.

Figure 2 shows the composite of all cases at three stages during the evolution of the storms. The figure includes 300-hPa as well as sea level gKE. Each composite is constructed by shifting the origin at each case and time to be at the center of the low. The trough axis location varies with height. The origin at 300 hPa is in the middle of each plot. The origin in the plots of sea level gKE is shifted by the average amount for all cases relative to the 300-hPa low; the shift is made for plotting purposes and comes after the composites are constructed. At 300 hPa, a well-defined maximum to the northwest of the low center migrates counterclockwise around the low center. During the mature stages the maximum moves to the south then to the east side of the low center. The location early in the development is to the west in all cases; though in several cases the maximum gKE is to the southwest of the low center. The location of gKE maximum in later stages is consistent with the development of the upper-level ridge ahead of the trough. The geostrophic winds are enhanced between that strong ridge and the trough in question. As a consequence of this asymmetric dependance upon the trailing or leading ridge, the maximum perturbation winds have different horizontal location at different levels.

Our gKE results may be compared with other studies, all those cited here use kinetic energy (KE). Direct comparison must be moderated, mainly by gradient versus geostrophic wind differences due to curvature. A jet

streak traveling down the west side of a strongly curved trough may weaken and disappear while a second maximum appears and strengthens on the east side. Pauley et al. (1996, Figs. 14–17) present an example of this effect. In contrast, the geostrophic winds would show a continuous propagation of the gKE maximum. Here, gKE is used to establish scale (primarily) and display a basic property (secondarily) of the cyclones. We believe that insensitivity to curvature makes gKE more useful for describing scale change than KE. The differences between total and geostrophic KE may not be important here because our technique does not emphasize the maximum gKE, but finds a radius whose circular average value is near the background level of gKE: this occurs where curvature is generally small. As for the basic property, we compared gKE and KE fields in cases A, G, and K for all times at 300 hPa. (These cases sample a wide range of trough shapes and scale changes.) The differences in structure were small. Within 1800 km of the trough center, the gKE and KE fields have average correlation of 0.86, with standard deviation 0.07. So, the KE maxima differed in size but were located very similarly in these 27 pairs. Hence, the location of strongest wind is emphasized here, not the magnitude.

The horizontal patterns of gKE at 300 hPa here evolve in a way similar to patterns for KE seen in other studies. For comparison, Sechrist and Dutton (1970) show a time sequence of KE for a cyclone developing over eastern North America. While they show KE on the 305-K potential temperature surface, the migration of KE maxima is generally similar to what we find in most cases as well as in the composite. In our cases, the individual perturbation gKE fields often have one prominent maximum. The gKE maximum corresponds to a jet streak as usually discussed in the synoptic literature. In some cases the KE maximum migrates around the upper trough from the SW to the SE side, much like the presentation in synoptic meteorology books (e.g., Carlson 1994, Fig. 10.4; Palmén and Newton 1969, Fig. 11.15; Bluestein 1993, Fig. 1.133). However, in other cases studied here, the streak moves differently: remains on the west side, continues migrating around the east side all the way to the NW side, or something else.

The KE structure varies between case studies such as Bettge et al. (1976), Robertson and Smith (1980), and Dare and Smith (1984). In Robertson and Smith (1980) two cyclones over North America are tracked; in one case the KE maximum (integrated from 200 to 400 hPa to get volume content) and jet streak are rather straight and remain on the south side of the upper trough; in their other case the KE content maximum is curved and appears to migrate counterclockwise around the trough. Dare and Smith (1984) show eddy (zonal mean deviation) KE and 300-hPa isotachs at 24-h intervals; there is one maximum at the start (on the west side) while a second maximum occurs on the east side at the two other times shown. A scale change is seen in Dare and Smith's case: between the middle and last time shown the separation between the two KE maxima increases (the upper and sea level troughs both broaden).

At sea level, the maximum gKE rotates farther around the low in a counterclockwise manner, ending up to the west of the low in the composite (see Fig. 2). The sea level gKE pattern is consistent with the development of the trailing surface high [linked to sinking behind the upper trough; e.g., Fig. 5 in Grotjahn (1996b)]. Close proximity to the surface low leads to stronger geostrophic winds in between the trailing high and the low.

The picture that emerges from this analysis is that the upper ridge ahead of the trough and trailing low-level ridge are required to generate the larger values in the gKE pattern. Hence, any theoretical treatment that attempts to isolate a single trough must include the leading upper high and trailing low-level high.

Compared with 300 hPa, the sea level gKE pattern is more annularly symmetric (as judged by the ratio of maximum to minimum value at the radius of the maximum). Another difference is that the KE grows much more at sea level than at upper level. Grotjahn (1996a) reports a consistent finding: the perturbation Z magnitude at 308 hPa increases slightly, while the perturbation Z at 899 hPa quadruples during development.

b. Circular average results

1) RADIAL DISTRIBUTION

Figure 3 shows the circular average gKE at 300 hPa, while Fig. 4 shows the corresponding sea level gKE. The composite average is plotted as a solid line. Boxes enclose the middle two quartiles (six cases) and the vertical lines show the extremes, both at 100-km intervals of radius. (Defining the boxes using standard deviations was judged inappropriate given the small sample size here.) Generally speaking, box midpoints agree quite well with the radius at which the 12-case composite gKE is largest. The 12-case average exceeds the box midpoint for the obvious reason that the data are skewed because gKE is nonnegative. On average, the peak at 300 hPa is at 800-km radius, while at sea level the peak is at 500 km. Also noteworthy is that the consistency between successive boxes improves as the storms intensify. This result suggests that from rather different early states the systems develop a more similar structure at later times. This view is consistent with our subjective impression when looking at individual maps.

The circular average gKE has peak value located between 600 and 1100 km over time in most *individual* cases at 300 hPa. In contrast, the surface geostrophic KE has peak value located typically between 450 and 650 km from the SLP center over time in the *individual* cases. As one consequence, the composite average shows a broader peak at 300 hPa than at sea level. Another factor is the narrower range of values at sea level than at 300 hPa (compare box lengths in Figs. 3c

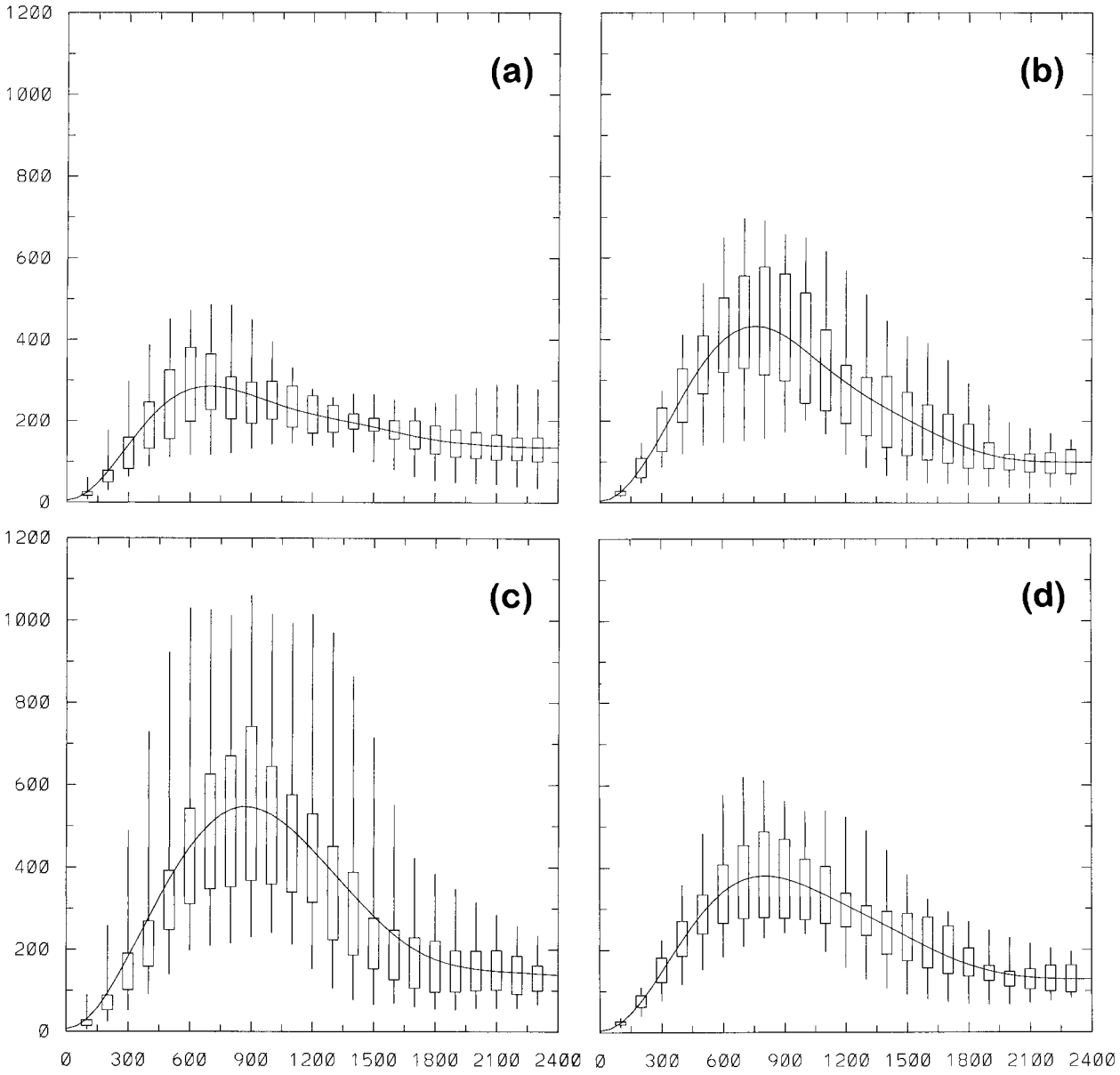

FIG. 3. Radial distribution of gKE at 300 hPa at the three stages (a)–(c) in the cyclone development as shown in Fig. 2 plus for all cases and times (d). The times chosen are (a) −1, (b) 0, and (c) +1.5 days for each case. Time 0 is a mature stage while time −1 is quite early in the cyclone development. The solid line depicts the composite average for the 12 cases. Quartiles are indicated using a ''box and whisker'' format; the box encloses the middle two quartiles (six cases) while the vertical lines define the extremes in the data. Units are $m^2 s^{-2}$.

and 4c). It is possible that some of this difference may arise from an imperfect perturbation calculation procedure at 300 hPa.

Even though the peak gKE values are often larger at 300 hPa, the circular average values at later times are greater at the surface (Figs. 3c and 4c) due to the greater annular symmetry in sea level gKE. (However, the largest midpoints of boxes enclosing the middle quartiles are similar at 300 hPa and sea level.)

2) SCALE CHANGES

For each system, the scale was calculated at each of the valid times and a scatterplot was produced showing time versus scale. Since the scale was defined from the intersection of the circular average gKE and a cutoff value, several choices were tested for the cutoff value. Due to differences in the magnitudes of the surrounding flow, a different cut off was used at 300 hPa than at sea

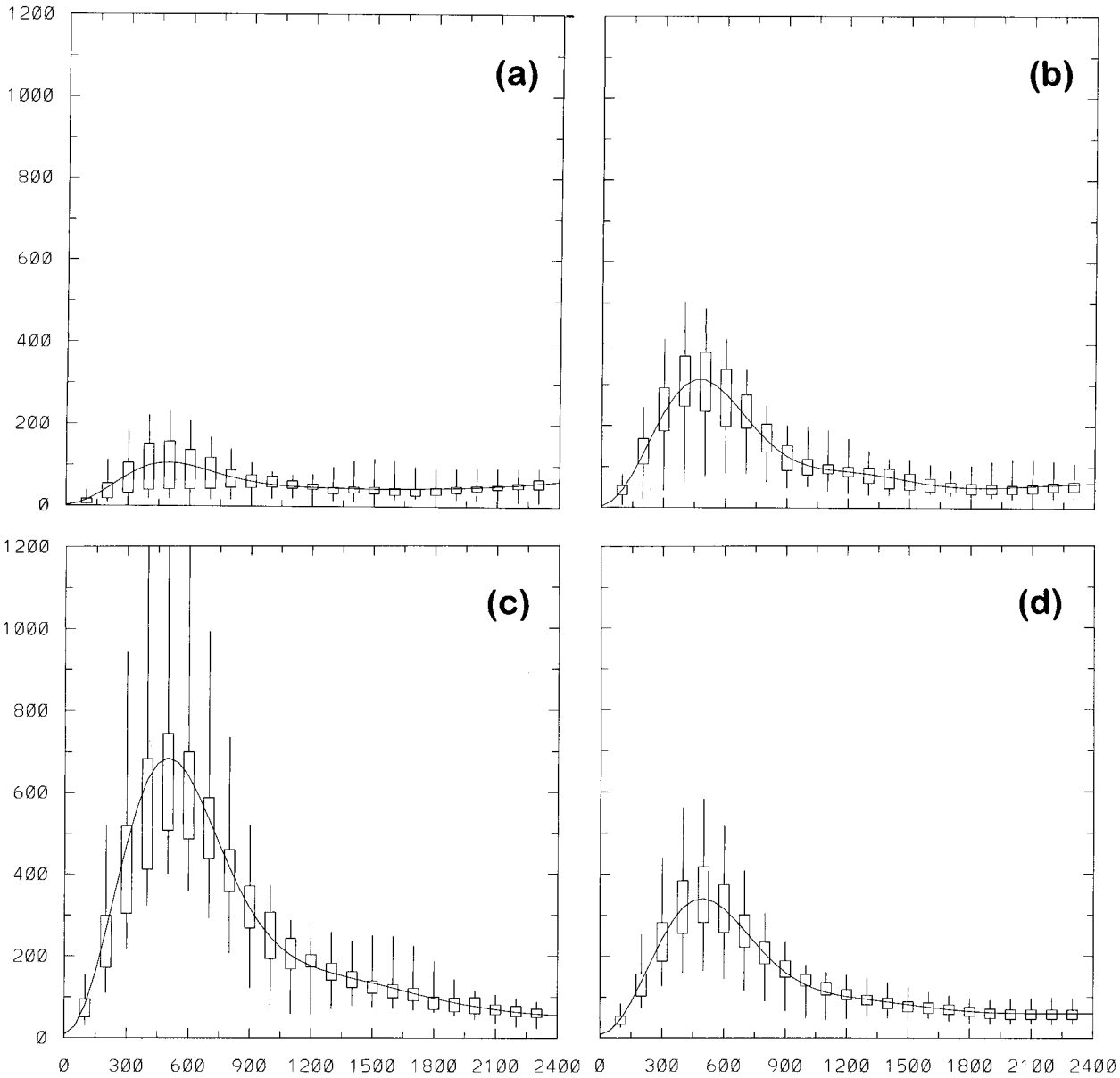

FIG. 4. Similar to Fig. 3 except for radial distribution of gKE deduced from sea level pressure.

level. Regression analysis statistics of each scatterplot (as done in GHC) help determine whether scale change at 300 hPa is statistically significant. At each level, plots show the raw scale as well as scale normalized to the value at the midpoint of each time sequence.

The scatterplot of 300-hPa scale versus time for a cutoff value of 250 $m^2\ s^{-2}$ is shown in Figs. 5a,c. The regression lines for the data points in Figs. 5a,c are also plotted. The regression lines have a slope, implying an increase in scale. Some readers may draw the subjective impression that our measure of scale increases as the lows develop. But as in GHC, we test whether the slope of the line is significantly different from a flat line. Hence, our null hypothesis is that there is no change in trough scale (extent). As in GHC, an appropriate test is the ''*F* test'' and as in GHC the 12 cases here contain at least 10 degrees of freedom. The *F*-test value for the raw data in Fig. 5a is 2.87, which is far below the necessary *F*-test value for passing with 99% confidence (10.04) or even 95% confidence (4.96). Varying the cutoff value up and down did not significantly alter the *F*-test value (2.64 for a cutoff value of 240 $m^2\ s^{-2}$ and 2.23 for a cutoff value of 260 $m^2\ s^{-2}$). Normalizing the scales (to account for differences in the average size of individual storms) is not sufficient to show a statistically significant scale change. For example, the *F* test for data in Fig. 5c is 5.05, which barely passes the 95% limit (4.96); however, using any other time for normalization

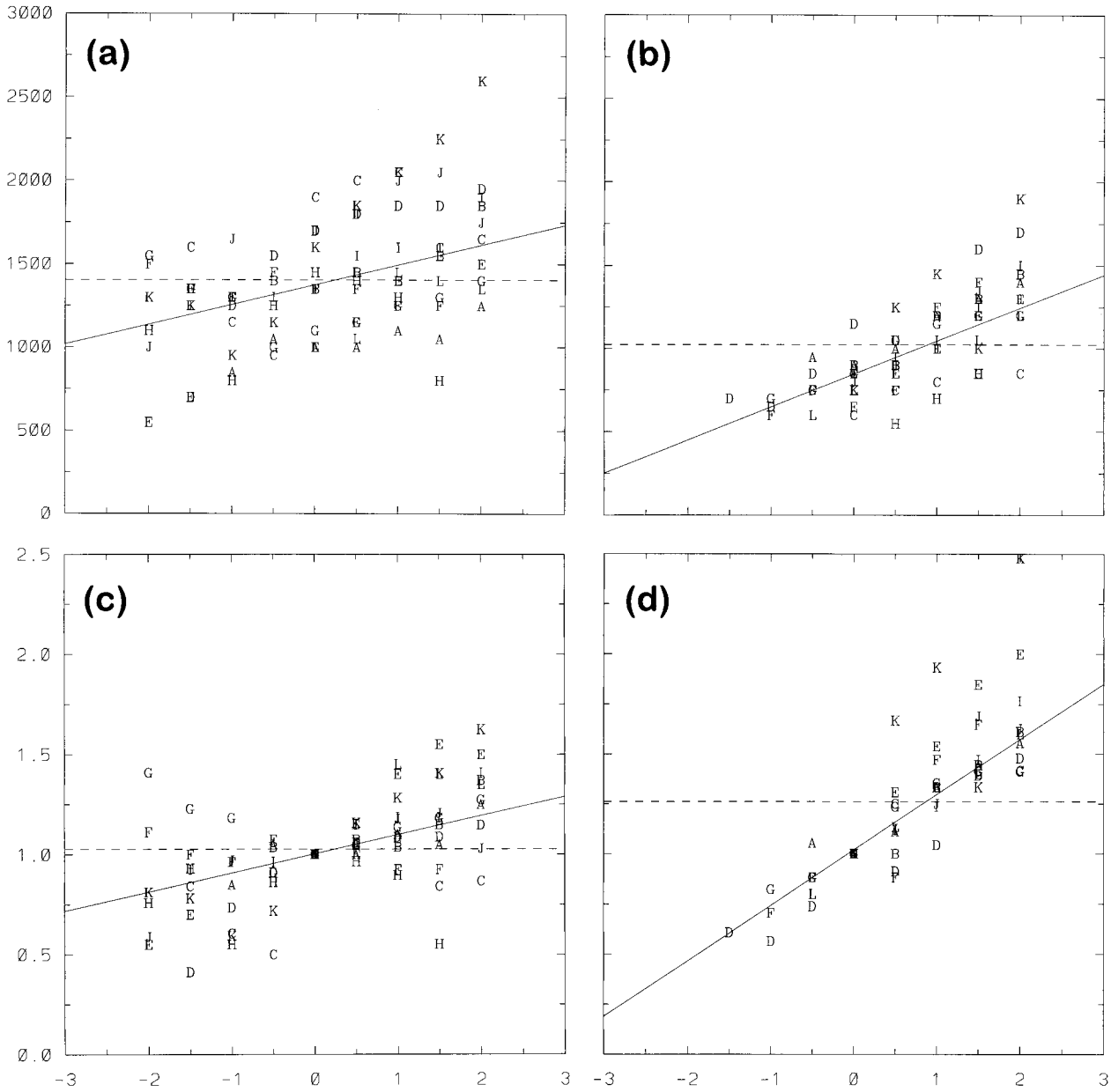

FIG. 5. Scatterplot of trough scale vs time for the 12 cases as deduced from the circular average gKE field. Raw data, in km: (a) at 300 hPa and (b) at sea level. Data normalized using the value at time 5: (c) at 300 hPa and (d) at sea level. Regression lines based on the data are also plotted. The time interval is in days relative to the midpoint of the time samples for each case. Only the sea level data have a statistically significant increase in the horizontal scale of the trough.

does not pass even this low limit. Hence, one cannot confidently conclude that there is evidence of scale growth at the 300 hPa level.

Circular average gKE scales from sea level pressure were calculated in order to compare results from the procedure herein with the results obtained from the wavelet analysis in GHC. Scales from the new procedure are plotted in Fig. 5b. The two procedures measure different things, so the magnitudes of the scales plotted here and in GHC are different. However, the trend in scale change seen in Figs. 5b,d is comparable with the trend seen in Figs. 2 and 3 of GHC. Since the *F* test applies to scale, not magnitude, one can compare the results for the two procedures. Defining scale from the circular average gKE field using a cutoff value of 180 $m^2\ s^{-2}$ obtained an *F*-test value of 11.61 from the raw data. This may be compared to a value of 14.59 from the wavelet analysis in GHC. Changing the cutoff value to 170 $m^2\ s^{-2}$ gave an *F*-test value of 12.17, and a cutoff value of 190 $m^2\ s^{-2}$ gave an *F*-test value of 12.28. All

of these values pass the 99% test. When the scales were defined using cutoff values of 170, 180, and 190 $m^2 s^{-2}$ and were normalized at the sixth time step (not shown), the *F*-test values were 22.12, 20.14, and 18.89, respectively. Normalizing the data to the sixth time step with wavelet analysis gave an *F*-test value of 24.17. Hence, the results obtained by examining the radial gKE for the surface cyclones verifies the increasing scale result found using wavelet analysis. The size of the scale change from early to late in the development is comparable to our prior study, the radial gKE scale roughly doubles over the course of the development.

Any definition of ''scale'' in the sense of the horizontal extent of a low pressure system is somewhat arbitrary. However, the emphasis here is upon the change in measured scale and not upon the specific scale. To that end, robustness of the change is assessed by recalculations using bracketing values for the cutoffs. A reviewer expressed an additional concern. The nascent troughs might just exceed the cutoff value; as a result, the scale might be initially defined by the location of the gKE peak, but not later. If the gKE peak did not change radial distance from the low center (actually it moves slightly closer) then the scheme might make an exaggerated estimate of scale increase. To avoid this concern, the reviewer suggested a scheme using a cutoff defined from the difference between peak and background values at each time. For example: the reviewer suggested that the cutoff be greater than the background value by 20% of the difference between peak and background gKE. This alternative scheme yielded results qualitatively similar to our standard scheme: At 300 mb the *F*-test values were 3.26 and 4.72 for the raw and normalized scales, respectively, and at the surface the values were 8.52 and 15.02. The statistics at 300 mb still fail to pass even a 95% test as in the standard method. At the surface, while the raw data falls below the 99% threshold, it still passes a 95% *F* test, and the normalized data still exceed the required value for the 99% *F* test. Such results should not be too surprising; these results are consistent with GHC; the procedure in GHC does not use any type of cutoff value.

The aggregate scales for the mature cyclones differ at upper and lower levels, being near 1200 km at sea level, but closer to 1700 km at 300 hPa. While comparison of the raw scale between levels depends on the cutoff value used, the location of the maximum gKE does not. The location of maximum gKE (in the aggregate) also differs between levels, ranging from 700 to 900 km over time for the low center at 300 hPa, but only 500 km from the sea level pressure center. Robertson and Smith (1980) calculate KE energy budgets in quasi-circular regions defined by the outermost closed SLP contour. These regions increase in size for the two cases they show and range between 18° and 22° (latitude) in diameter—a size similar to the scales identified here. Bullock and Johnson (1971) and Johnson (1970) also examine energy budgets; they use a cylinder centered on the surface low position having 1700-km radius. Johnson and Hill (1987) use cylindrical volumes (4.5° and 10.5° radius) for a ''Mediterranean'' cyclone. Unfortunately, none of these studies show horizontal, nor azimuthal, averages of KE.

The trend in the measure of scale (storm extent measured to a cutoff value of gKE) used here differs from the trend in the location of the maximum annular average gKE. One might be concerned that our measure of scale is actually identifying the emergence of a (fixed, say) large-scale low from a background level of gKE as that low gains amplitude. A metaphor for the different trends in SLP scale deduced using gKE maximum versus a cutoff value might be a submarine emerging from underwater where sea level is the background KE. That analogy is consistent with no change in the radius of maximum KE while at the same time an increase in storm extent as measured here. Such an analogy likely does *not* apply. Visual inspection of the horizontal SLP pattern in every case finds small distances between successive highs and lows early in the development followed by much larger gaps later on. (One might argue that the Mexican hat wavelet results in GHC rule out the ''submarine analogy'' by emphasizing this separation.) On the other hand, visual inspection of the 300-hPa gKE and *Z* fields does *not* show that type of change seen in SLP. The separation distance does not change in a systematic way at 300 hPa, in part due to the amplification of the leading upper-level ridge (presumably in response to vertical motion ahead and above the surface low).

Close inspection of Fig. 4 suggests another measure of storm extent: tracking the point where there is a subtle change of slope in the composite average. The location of that point seems to increase from the earlier to the later times shown (near 900 km at time 5; near 1100 km at time 8). We do not see a similar trend in a slope change near 1900 km in the 300-hPa level data (Fig. 3). So, in terms of the upper trough, one's subjective impression is confirmed by the objective technique used here: no significant scale change.

4. Conclusions

The primary goal of this study was to investigate whether large increases of frontal cyclone horizontal extent seen in sea level pressure fields are accompanied by similar scale changes at upper levels. Here, the horizontal extent of a frontal cyclone is referred to as its ''scale.'' In an earlier study, GHC found that the SLP trough nearly doubled in size as it grew to a mature stage. To examine upper levels a different technique was needed than that used in GHC. The technique adopted here uses geostrophic perturbation kinetic energy. Our technique deduces cyclone scale from the circular average of gKE as a function of radial distance from the low center. To understand the context behind the scales defined here, the general properties of the KE field are

shown at the upper and lower troposphere both using composite and circularly averaged representations. Our technique was also applied to sea level pressure to check how well the new technique compares with the wavelet technique used by GHC.

As far as scale change is concerned, a statistically significant increase is found using the sea level gKE field (Figs. 5b,d) consistent with the GHC analysis of SLP. Scatterplots of 300-hPa level data (Figs. 5a,c) may create the impression of increasing scale but the change seen is not statistically significant. While comparison of the raw scale between levels depends on the cutoff value used, the location of the maximum gKE does not. The distances estimated for the scale of the system as a whole and for the radial distance to the peak gKE are both much larger at the upper level than at sea level, even after the doubling of the sea level extent of the whole system.

The picture that emerges from this analysis is that certain nearby highs are required to generate the larger values of the gKE pattern. Hence, any theoretical treatment that attempts to isolate a single trough must include the leading upper ridge and trailing low-level ridge. GHC point out that several published theoretical studies show linear solutions that appear to increase in scale downstream. It is outside the scope of this study to assess a theoretical issue, but scale change may be an important feature that is missing from most theoretical studies of cyclogenesis.

The circular average gKE pattern as mapped by the middle quartiles of the cases shows more consistency between adjacent radii at later stages of development than prior to development. This result suggests that from rather different early states the systems develop a more similar structure at later times. This view is consistent with our subjective impression when looking at individual maps. One example of a consistent structure that arises from varied initial states is an unstable normal mode, a result that may be important to the theoretical understanding of cyclogenesis.

Acknowledgments. The authors acknowledge generous support by the National Science Foundation through Grant ATM-96-15316.

REFERENCES

Bettge, T. W., P. J. Smith, and D. P. Baumhefner, 1976: A comparison of kinetic energy budget analysis derived from the NCAR GCM and observed data. *Mon. Wea. Rev.,* **104,** 1242–1254.

Bluestein, H. B., 1993: *Synoptic-Dynamic Meteorology in Midlatitudes.* Vol. II. *Observations and Theory of Weather Systems.* Oxford University Press, 594 pp.

Bullock, B. R., and D. R. Johnson, 1971: The generation of available potential energy by latent heat release in a mid-latitude cyclone. *Mon. Wea. Rev.,* **99,** 1–14.

Dare, P. M., and P. J. Smith, 1984: A comparison of observed and model energy balance for an extratropical cyclone system. *Mon. Wea. Rev.,* **112,** 1289–1308.

Carlson, T. N., 1994: *Mid-Latitude Weather Systems.* Routledge, 507 pp.

Grotjahn, R., 1996a: Composite trough evolution of selected west Pacific extratropical cyclones. *Mon. Wea. Rev.,* **124,** 1470–1479.

——, 1996b: Vorticity equation terms for extratropical cyclones. *Mon. Wea. Rev.,* **124,** 2843–2858.

——, D. H. Hodyss, and C. Castello, 1999: Do frontal cyclones change size? Observed widths of North Pacific lows. *Mon. Wea. Rev.,* **127,** 1089–1095.

Johnson, D. R., 1970: The available potential energy of storms. *J. Atmos. Sci.,* **27,** 727–741.

——, and D. K. Hill, 1987: Quasi-Lagrangian diagnostics of a Mediterranean cyclone: Isentropic results. *Meteor. Atmos. Phys.,* **36,** 118–140.

Nielsen, J. W., and R. M. Dole, 1992: A survey of extratropical cyclone characteristics during GALE. *Mon. Wea. Rev.,* **120,** 1156–1167.

Palmén, E., and C. W. Newton, 1969: *Atmospheric Circulation Systems, Their Structure and Physical Interpretation.* Academic Press, 603 pp.

Pauley, P., N. Baker, and E. Barker, 1996: An observational study of the ''Interstate 5'' dust storm case. *Bull. Amer. Meteor. Soc.,* **77,** 693–720.

Robertson, F. R., and P. J. Smith, 1980: The kinetic energy budgets of two severe storm producing extratropical cyclones. *Mon. Wea. Rev.,* **108,** 127–143.

Sechrist, F. S., and J. A. Dutton, 1970: Energy conversions in a developing cyclone. *Mon. Wea. Rev.,* **98,** 354–362.